

Article

Heteroligand α -Diimine-Zn(II) Complexes with O,N,O'- and O,N,S-Donor Redox-Active Schiff Bases: Synthesis, Structure and Electrochemical Properties

Ivan V. Smolyaninov ^{1,*} , Andrey I. Poddel'sky ² , Daria A. Burmistrova ^{1,*}, Julia K. Voronina ³ , Nadezhda P. Pomortseva ¹, Vasilii A. Fokin ¹, Ekaterina D. Tselukovskaya ^{3,4}, Ivan V. Ananyev ³, Nadezhda T. Berberova ¹ and Igor L. Eremenko ³

¹ Department of Chemistry, Astrakhan State Technical University, 16 Tatisheva Str., 414056 Astrakhan, Russia

² G.A. Razuvaev Institute of Organometallic Chemistry, Russian Academy of Sciences, 49 Tropinina Str., 603137 Nizhny Novgorod, Russia

³ Kurnakov Institute of General and Inorganic Chemistry, Russian Academy of Sciences, Leninskii prospekt 31, 119071 Moscow, Russia

⁴ Faculty of Chemistry, National Research University Higher School of Economics, 20 Myasnitskaya Str., 101000 Moscow, Russia

* Correspondence: ivsmolyaninov@gmail.com (I.V.S.); burmistrova.da@gmail.com (D.A.B.)



Citation: Smolyaninov, I.V.; Poddel'sky, A.I.; Burmistrova, D.A.; Voronina, J.K.; Pomortseva, N.P.; Fokin, V.A.; Tselukovskaya, E.D.; Ananyev, I.V.; Berberova, N.T.; Eremenko, I.L. Heteroligand α -Diimine-Zn(II) Complexes with O,N,O'- and O,N,S-Donor Redox-Active Schiff Bases: Synthesis, Structure and Electrochemical Properties. *Molecules* **2022**, *27*, 8216. <https://doi.org/10.3390/molecules27238216>

Academic Editors: Marina Fonari and Rodica Olar

Received: 29 October 2022

Accepted: 22 November 2022

Published: 25 November 2022

Publisher's Note: MDPI stays neutral with regard to jurisdictional claims in published maps and institutional affiliations.



Copyright: © 2022 by the authors. Licensee MDPI, Basel, Switzerland. This article is an open access article distributed under the terms and conditions of the Creative Commons Attribution (CC BY) license (<https://creativecommons.org/licenses/by/4.0/>).

Abstract: A number of novel heteroligand Zn(II) complexes (1–8) of the general type (Lⁿ)Zn(NN) containing O,N,O'-, O,N,S-donor redox-active Schiff bases and neutral N,N'-chelating ligands (NN) were synthesized. The target Schiff bases LⁿH₂ were obtained as a result of the condensation of 3,5-di-*tert*-butyl-2-hydroxybenzaldehyde with substituted *o*-aminophenols or *o*-aminothiophenol. These ligands with combination with 2,2'-bipyridine, 1,10-phenanthroline, and neocuproine are able to form stable complexes upon coordination with zinc(II) ion. The molecular structures of complexes 4·H₂O, 6, and 8 in crystal state were determined by means of single-crystal X-ray analysis. In the prepared complexes, the redox-active Schiff bases are in the form of doubly deprotonated dianions and act as chelating tridentate ligands. Complexes 6 and 8 possess a strongly distorted pentacoordinate geometry while 4·H₂O is hexacoordinate and contains water molecule coordinated to the central zinc atom. The electrochemical properties of zinc(II) complexes were studied by the cyclic voltammetry. For the studied complexes, O,N,O'- or O,N,S-donor Schiff base ligands are predominantly involved in electrochemical transformations in the anodic region, while the N,N'-coordinated neutral nitrogen donor ligands demonstrate the electrochemical activity in the cathode potential range. A feature of complexes 5 and 8 with sterically hindered *tert*-butyl groups is the possibility of the formation of relatively stable monocation and monoanion forms under electrochemical conditions. The values of the energy gap between the boundary redox orbitals were determined by electrochemical and spectral methods. The parameters obtained in the first case vary from 1.97 to 2.42 eV, while the optical band gap reaches 2.87 eV.

Keywords: redox-active ligand; tridentate Schiff base; zinc; crystal structure; X-ray; cyclic voltammetry

1. Introduction

The formation of organic/organoelemental hybrid molecules containing several types of redox-active ligands requires the development of new approaches characterized by a high efficiency and suitability for preparation of substances with desired properties. One of the promising directions in the synthesis of coordination compounds is the assembly of target complexes via the combination of various redox-active molecular blocks. To solve this problem, it is important to combine several different types of ligands, for example, O,N,O'-, O,N,S-tridentate Schiff bases and N,N'-chelating ligands.

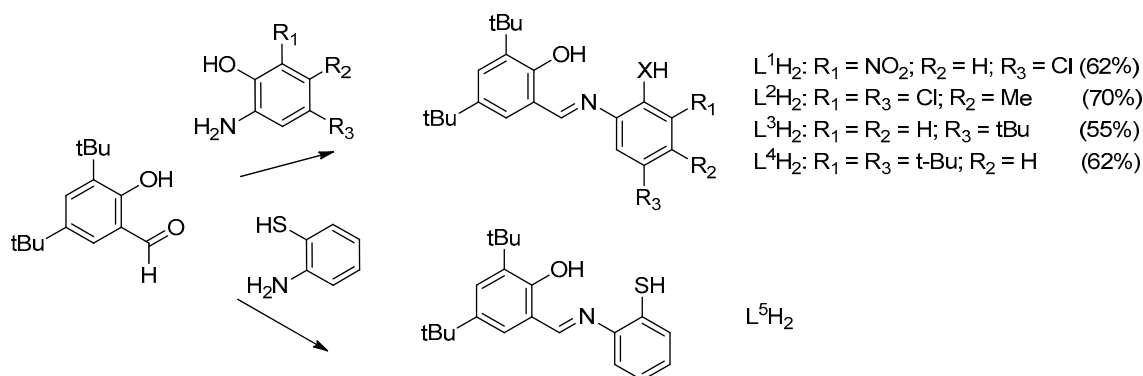
Zinc compounds are the basis for creating substances with light-emitting properties [1]. Zinc complexes represent one of the unique classes of fluorescent compounds that have

wide biological applications [2]. Zinc complexes with O,N,O'-donor ligands possess antibacterial, antioxidant, and antitumor activity [3–6]. At the same time, mixed-ligand zinc complexes with bipyridine ligands and diketonates, tropolones are also characterized by the high cytotoxicity against cancer cells [7,8]. Such interest in the combination of bioactive metal-zinc and natural compounds (curcumin, hydroxyflavones, etc.), as well as molecules with an extended planar aromatic system, which are suitable candidates for intercalation into the DNA structure, is caused by the high antitumor activity of such substances [9]. In particular, zinc complexes with phenanthroline and Schiff bases exhibit cytotoxicity and selectivity towards cancer cells, and are also characterized by the possibility of forming reactive oxygen species and inducing lipid peroxidation [10]. In addition to cytotoxic properties, zinc(II) compounds with various ligands exhibit antioxidant and luminescent properties [11,12].

Along with neutral nitrogen-containing ligands, bi- (O,N-, S,N-), tridentate (O,N,O'-, O,N,N'-, etc.) ligands are widely used for the design of zinc(II) compounds with luminescent and fluorescent properties [13–18]. A sufficient number of complex compounds containing transition metals are known. For O,N,S-coordinated Schiff bases [19–23]. For zinc derivatives, mainly bis-chelate complexes with N,S-ligands were obtained [24–26]. Only a few examples of zinc complexes with tridentate O,N,S-ligands are known [27–29]. The introduction of donor/acceptor substituents and the variation of heteroatoms in Schiff bases will affect the spectral and electrochemical properties. Due to the limited valence states available for the metal under study (zinc), the combination of zinc ions with molecular blocks capable of changing their oxidation state will increase the number of possible redox forms of the complexes which in turn can lead to the appearance of new properties.

In this regard, the aim of the work is the synthesis of new heteroligand zinc complexes containing neutral N,N'-chelating ligands, such as 2,2'-bipyridine (Bipy), 9,10-phenanthroline (Phen), 2,9-Dimethyl-1,10-phenanthroline (Neocuproine, Neo) and redox-active tridentate O,N,O'- or O,N,S-donor Schiff bases LⁿH₂ (Scheme 1).

The presence of diverse redox-active ligands determines the possibility of their participation in electrochemical transformations, depending on their ability to donate/accept electrons. A distinctive feature of the synthesized zinc(II) complexes is the absence of the necessity to involve metal in a chemical process since redox-active ligands can serve as a reservoir for storing or transferring electrons. Moreover, there are ample opportunities for fine-tuning the redox properties of ligands by varying substituents. The Schiff bases used in the present work were obtained by the condensation of 3,5-di-*tert*-butyl-2-hydroxybenzaldehyde with functionalized *o*-aminophenols and *o*-aminothiophenol. They are able to form stable complex compounds upon coordination with zinc ions. The presence of substituents stabilizing various redox forms in the structure of ligands makes it possible to evaluate the stability of the oxidized/reduced forms of their complexes using electrochemical methods and to determine the energy gap between the boundary redox orbitals.



Scheme 1. Synthesis of Schiff bases L^{1–5}H₂.

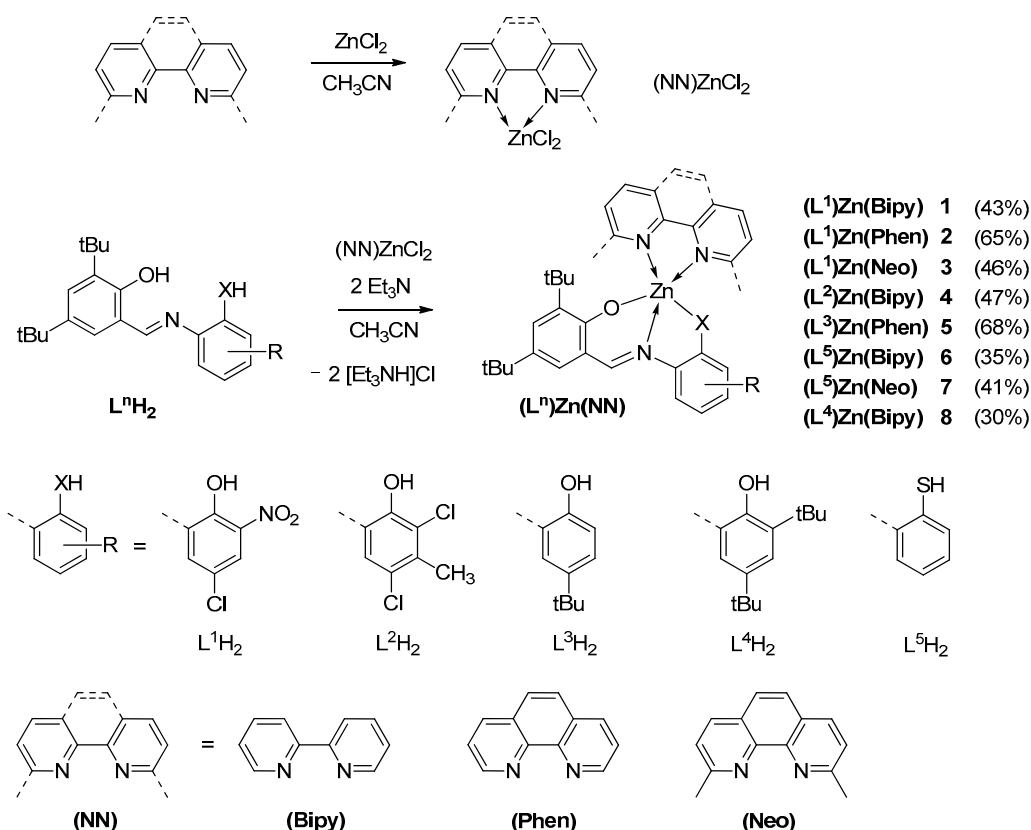
2. Results and Discussion

2.1. Synthesis and Characterization

The reaction of 3,5-di-*tert*-butyl-2-hydroxybenzaldehyde with *o*-aminophenols with various donor or acceptor substituents as well as with *o*-aminothiophenol in refluxing methanol leads to the formation of Schiff bases L^1H_2 - L^5H_2 (Scheme 1).

The preparative yield of L^1H_2 - L^4H_2 was from 55% to 70%. Compounds have been characterized by means of 1H and $^{13}C\{^1H\}$ NMR-, IR-spectroscopy, and mass-spectrometry.

Synthesis of zinc(II) complexes **1–8** was carried out as the exchange reaction between the corresponding Schiff base and $ZnCl_2$ in the presence of α -diimines and triethylamine as deprotonated agent (Scheme 2).



Scheme 2. Synthesis of zinc complexes **1–8** of the type $(L^{1-5})Zn(NN)$.

The synthesis was performed in anaerobic conditions to prevent side oxidation processes of ligands. Compounds **1–8** were isolated as orange or red-orange crystalline powders with yields up to 68%. Complexes **1–8** are air-stable in the solid state. Compounds have been characterized by means of IR, 1H and $^{13}C\{^1H\}$ NMR spectroscopy (Figures S1–S15), C,H,N-elemental analysis. The spectral and elemental analysis data confirm the composition of complexes. The X-ray suitable crystals of **6**, **8**· CH_3CN were grown by the prolonged crystallization of the corresponding powders from acetonitrile solutions under reduced pressure, while the crystals **4**· H_2O · CH_3CN —by the slow evaporation of acetonitrile on air.

2.2. X-ray Structures

The molecular structures of complexes **4**· H_2O (Figure 1), **6** (Figure 2), and **8** (Figure 3) in crystals (**4**· H_2O · CH_3CN , **6**, and **8**· CH_3CN) were determined by using single crystal X-ray diffraction method. The crystal cell of **6** contains two crystallographically independent molecules **6A** and **6B** with similar characteristics, and below we consider **6A** only.

The O,N,O'- or O,N,S-tridentate ligands in complexes contain two six-membered rings, which are linked by the C=N double bond. The ring C(1–6) in complexes **4**·H₂O, **6**, and **8** is aromatic with the average C–C bond length of 1.397, 1.395 and 1.402 Å, respectively (Table 1). The second ring C(8–13) is more distorted with av. C–C bond of 1.409, 1.408 and 1.405 Å, respectively. The C7–N3 bonds of 1.298(4), 1.292(4) and 1.279(4) Å are double in conjugation with C(8–13) carbon ring. The C–O bonds—C1–O1 (1.311(3) Å) and C2–O8 (1.294(3) Å) in **4**·H₂O; C8–O1 (1.310(4) Å) in **6**; C1–O1 (1.326(3) Å) and C2–O8 (1.307(3) Å) in **8**—are ordinary and correspond to the related C–O bonds in different chelated phenolato complexes [30–35]. In general, these bond lengths correspond to these bonds in different zinc complexes with related O,N,O'- or O,N,S-tridentate ligands: the C–O bonds in such complexes are in the range of 1.300–1.325 Å in five-membered metallocycle and 1.315–1.350 Å in six-membered metallocycles [36–42]. The C–N distances in the earlier reported complexes are 1.280–1.300 Å. The Zn–O and Zn–N bonds in **4**·H₂O, **6**, and **8** also typical for such zinc compounds (Zn–O, 1.960–2.105 Å; Zn–N, 2.020–2.090 Å). However, we should note that the overwhelming number of zinc complexes with these O,N,O'- or O,N,S-tridentate ligands are bi- and polynuclear, where the oxygen of phenolate group behaves as a μ -oxo linker. As a result, the Zn–O and C–O bonds of such moiety are elongated, being closer to the upper limits of the indicated ranges of these bond distances.

Crystals of complex **4** were grown from acetonitrile solution on air as **4**·H₂O·CH₃CN, where a water molecule is coordinated to the central zinc atom (Figure 1).

Table 1. The selected bond lengths (Å) in **4**·H₂O, **6**, and **8** according to the X-ray analysis data.

Bond	4 ·H ₂ O	6A/6B	8
Zn1–N1	2.189(2)	2.181(3)/2.158(3)	2.109(2)
Zn1–N2	2.148(2)	2.128(3)/2.151(3)	2.100(2)
Zn1–N3	2.086(2)	2.084(3)/2.079(3)	2.062(2)
Zn1–O1	2.0634(19)	1.951(2)/1.952(3)	1.985(2)
Zn1–O2	2.0055(19)	-	1.998(2)
Zn1–O3	2.238(2)	-	-
Zn1–S1	-	2.3149(10)/2.3219(10)	-
C1–O1	1.311(3)	-	1.326(3)
C8–O2	1.294(3)	-	1.307(3)
C8–O1	-	1.310(4)/1.299(4)	-
C2–N3	1.412(4)	1.422(4)/1.413(5)	1.426(4)
C7–N3	1.298(4)	1.292(4)/1.292(5)	1.279(4)
C1–S1	-	1.766(4)/1.769(4)	-
C1–C2	1.425(4)	1.404(5)/1.415(5)	1.408(4)
C1–C6	1.411(4)	1.402(5)/1.395(5)	1.427(4)
C2–C3	1.387(4)	1.399(5)/1.389(5)	1.392(4)
C3–C4	1.382(4)	1.387(5)/1.389(5)	1.392(4)
C4–C5	1.390(4)	1.391(5)/1.388(6)	1.399(4)
C5–C6	1.386(4)	1.388(5)/1.383(5)	1.396(4)
C7–C13	1.433(4)	1.434(5)/1.438(5)	1.442(4)
C8–C9	1.443(4)	1.440(5)/1.440(5)	1.439(4)
C8–C13	1.434(4)	1.431(5)/1.431(5)	1.435(4)
C9–C10	1.384(4)	1.376(5)/1.383(5)	1.388(4)
C10–C11	1.412(4)	1.422(5)/1.404(5)	1.408(4)
C11–C12	1.369(4)	1.361(5)/1.369(5)	1.367(4)
C12–C13	1.413(4)	1.417(5)/1.419(5)	1.395(4)

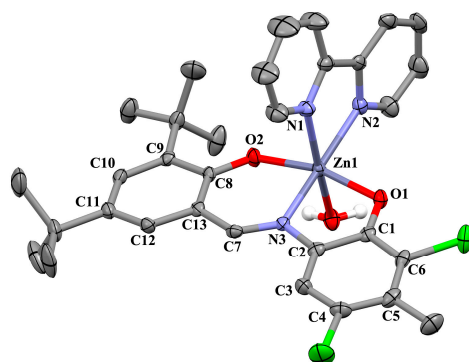


Figure 1. The molecular structure of $4 \cdot \text{H}_2\text{O}$ in crystals $4 \cdot \text{H}_2\text{O} \cdot \text{CH}_3\text{CN}$. The hydrogen atoms except for water are omitted for clarity. The ellipsoids of 50% probability.

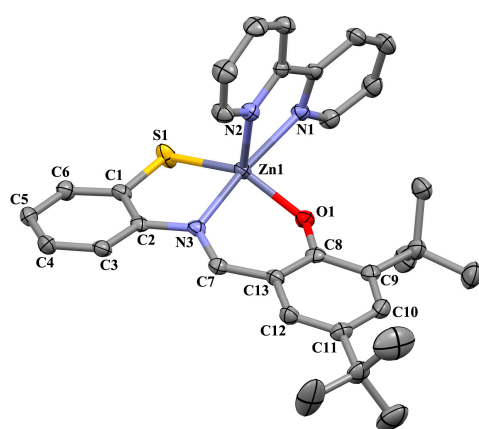


Figure 2. The X-ray structure of **6**. The hydrogen atoms are omitted for clarity. The ellipsoids of 50% probability.

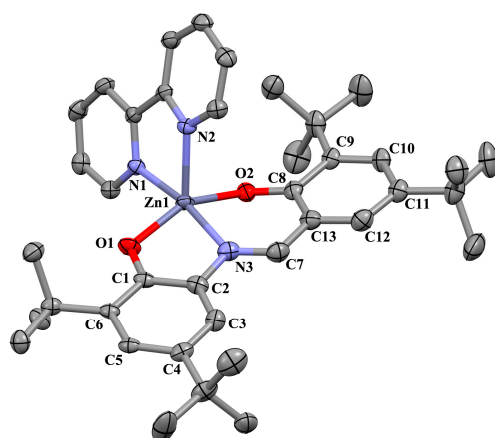


Figure 3. The X-ray structure of **8**. The hydrogen atoms are omitted for clarity. The ellipsoids of 50% probability.

The Zn1 atom in **4** adopts a distorted octahedral environment. The central Zn1 atom is disposed slightly of the planes of the chelating ligand: the distance “Zn1 ... plane O1C(1-6)N3” is 0.052 Å, and the distance “Zn1 ... plane O2C(8-13)C1N3” is 0.179 Å. The chelating cycles are not planar: the bent angle of the 5-membered chelate cycle along line O1 ... N3 is 3.26°, while the bent angle of the 6-membered chelate cycle nearly along line O2 ... N3 is 8.38°.

Complexes **6** and **8** possess a strongly distorted pentacoordinate geometry of the coordination center, which is intermediate between trigonal bipyramid and tetragonal

pyramid based on the formal parameter τ ($\tau = 1$ for ideal trigonal bipyramid and $\tau = 0$ for an ideal tetragonal pyramid [43]): $\tau = 0.52$ and 0.56 for **6A** and **6B**, and $\tau = 0.29$ for **8**. The atoms O1, S1 in **6** or the atoms O1, O2 in **8**, and one of the nitrogen atoms N2 of the N,N'-bipyridine lie in the equatorial plane of the complex molecule.

The tridentate ligands in these pentacoordinate complexes **6** and **8** are distorted more significantly as compared with hexacoordinated complex **4**·H₂O (Figure 4). The central zinc atoms are located out of the planes of chelating fragments of tridentate ligands: the distance “Zn1 ... plane S1C(1–6)N3” is 0.436 \AA , the distance “Zn1 ... plane O1C(8–13)C7N3” is 0.613 \AA in **6A**, and, respectively, 0.143 \AA , 0.664 \AA in **8**. The angle between the planes formed by the atoms O1, C8, C13, C7, N3 and by the atoms O1, N3, Zn1 (which may be considered as the bent angle of the 6-membered chelate cycle along line O1 ... N3) is 22.43° in **6A**, that is close to the corresponding angle 24.00° between the planes formed by the atoms O2, C8, C13, C7, N3 and by the atoms O2, N3, Zn1 in **8**. At the same time, the angle between the planes formed by the atoms S1, C1, C2, N3 and by the atoms S1, N3, Zn1 (which may be considered as the bent angle of the 5-membered chelate cycle along line S1 ... N3) in **6A** is 15.78° , which is remarkably more than the related angle between the planes formed by the atoms O1, C1, C2, N3 and by the atoms O1, N3, Zn1 in **8** of 6.52° .

The presence of a large number of the centres of hydrogen binding leads to the fact that the main structural units in crystal **4** are centrosymmetric H-dimers (Table S1) connected by $\pi \dots \pi$ interactions into infinite chains that form a three-dimensional grid due to weak CH ... O and CH ... π interactions (Figure S16). There are no classical hydrogen binding donors in the compound **6**, therefore, the main structure-forming interaction in these crystals are $\pi \dots \pi$, leading to the formation of ribbons interconnected by weak van der Waals interactions (Figure S17). Compound **8** not only lacks hydrogen binding donors, but also the formation of $\pi \dots \pi$ interactions is hindered by volumetric tert-butyl substituents. The crystals of this compound are formed only due to weak CH ... O and CH ... π interactions and consist of corrugated layers parallel to the *c*0*b* plane (Figure S18).

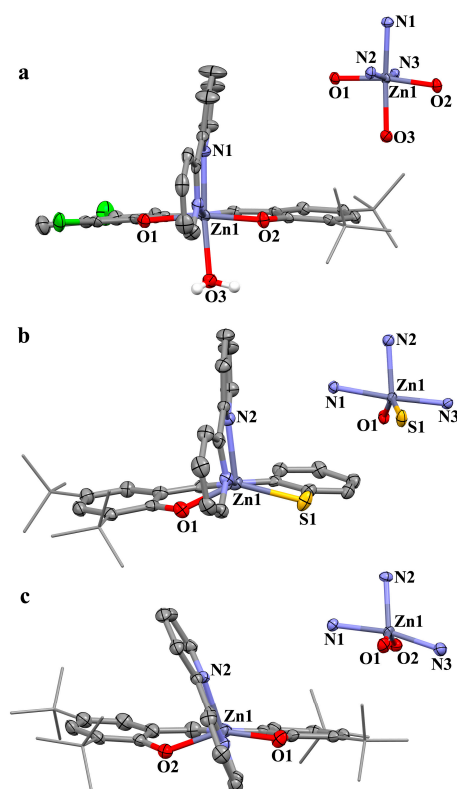


Figure 4. The views on the molecules and inner coordination spheres of **4**·H₂O (a), **6** (b), and **8** (c) along the bond Zn1–N3. The ellipsoids of 50% probability. The hydrogen atoms are omitted (except for H₂O in **4**·H₂O), and the tert-butyl groups are given as capped sticks.

2.3. Cyclic Voltammetry

The electrochemical behaviour of zinc complexes 1–8 was studied by cyclic voltammetry in dichloromethane solutions using a GC working electrode (Table 2).

Table 2. The CV data for 1–8 (CH_2Cl_2 , GC, 0.1M nBu_4ClO_4 , $C = 2 \times 10^{-3}$ M, Ar, vs. Ag/AgCl/KCl (sat.)).

Compound	$E^{\text{ox}1}_{1/2}$, V	I_c/I_a	$E^{\text{ox}2}$, V	$E^{\text{red}1}_{1/2}$, V	I_a/I_c	$E^{\text{red}2}_p$, V	ΔE_{el} , eV
1	0.87	0.7	1.40	−1.49 *	-	−1.74 *	2.42
2	0.87	0.8	1.23	−1.50 *	-	−1.72 *	2.44
3	0.92	1.0	1.43	−1.40 *	-	−1.70 *	2.38
4	0.70 *	-	0.86	−1.48	0.4	-	2.18
5	0.46	0.6	1.09	−1.55	0.4	-	2.01
6	0.77 *	-	1.10	−1.56	0.8	-	2.38
7	0.73 *	-	1.24 **	−1.62	0.7	-	2.38
8	0.41	1.0	0.77	−1.56	0.7	-	1.97

*—the peak potential; **—the value of potential $E^{\text{ox}2}_{1/2}$.

2.3.1. Oxidation

The electrochemical oxidation of complexes 1–8 proceeds in two or three successive anodic stages (Figure 5). For complexes 1–3, 5, and 8, the first anodic peak is quasi-reversible and one-electron, indicating the formation of monocationic particles relatively stable over the CV experiment time (Figure 6, Figures S19, S21 and S27).

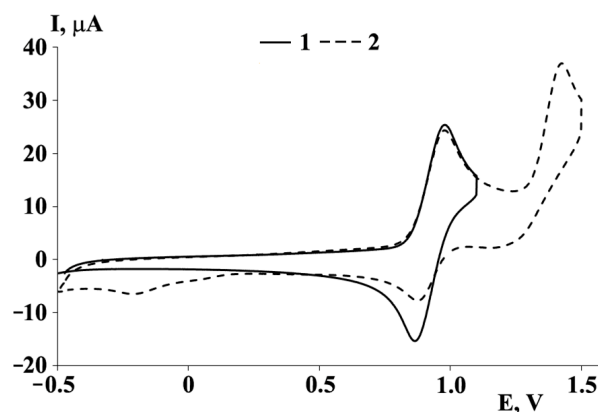


Figure 5. Cyclic voltammograms of 3: the potential switch from −0.50 to 1.10 V (curve 1); the potential switch from −0.5 to 1.5 V (curve 2) (CH_2Cl_2 , $C = 2$ mmol, 0.1 M TBAP, scan rate $200 \text{ mV} \cdot \text{s}^{-1}$).

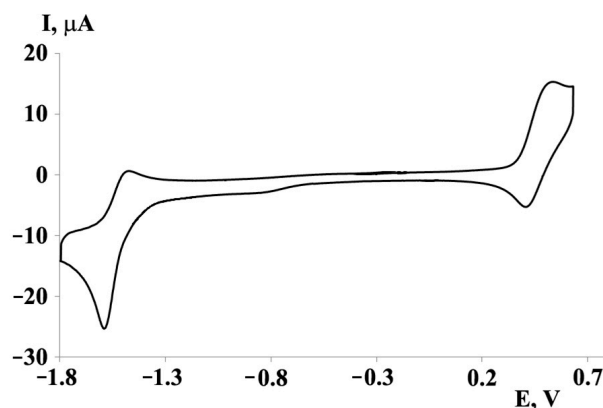
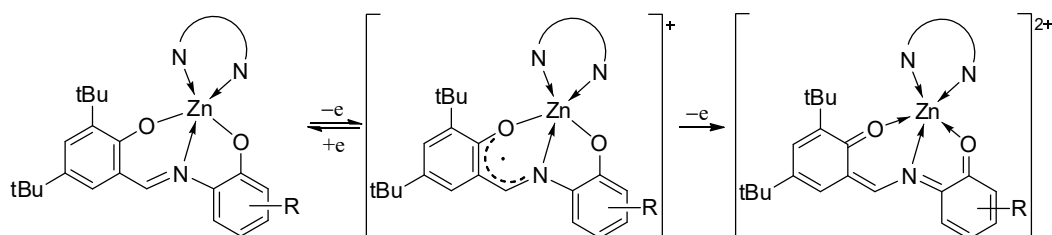


Figure 6. Cyclic voltammogram of 5 the potential switch from 0.63 to −1.80 V (CH_2Cl_2 , $C = 2$ mmol, 0.1 M TBAP, scan rate $200 \text{ mV} \cdot \text{s}^{-1}$).

Based on the values of current ratios, monocationic complexes formed during the electrooxidation of compounds **3** and **8**, containing substituents in the positions of 3,5-aromatic rings in Schiff bases, have the highest stability. The second oxidation stage for complexes **1–3**, **5**, and **8** is irreversible, which suggests the formation of an unstable dication intermediate. An increase in the potential sweep range with the capture of the second anodic peak leads to a decrease or complete loss of the reversibility of the first oxidation stage (Figure 5 and Figure S21), which indicates the occurrence of a chemical stage—partial decoordination of the doubly oxidized form of the ligand (Scheme 3).



Scheme 3. Two successive electrochemical oxidation stages for complexes **1–3**, **5**, and **8**.

Replacing the O,N,O'-ligand with O,N,S-ligand (in compounds **6**, **7**) or the nitro group with a chlorine atom (in complex **4**) contributes to the destabilization of the monocationic complex generated during electrooxidation, which is expressed in the irreversibility of the first stage of oxidation (Figure 7, Figures S22 and S25). The second anodic peak for compounds **4** and **6** is also irreversible. The presence of a pronounced reversibility for the second anodic peak ($I_c/I_a = 0.6$) on the CV of complex **7** distinguishes it from other compounds.

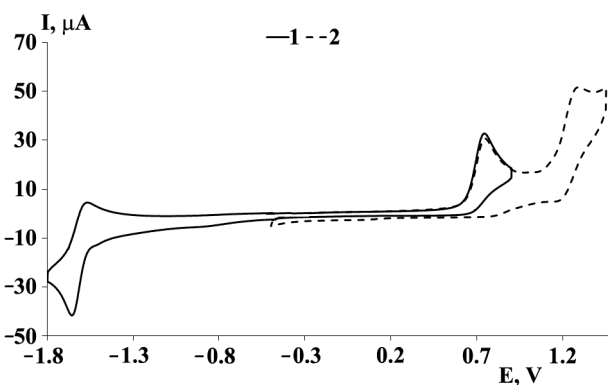
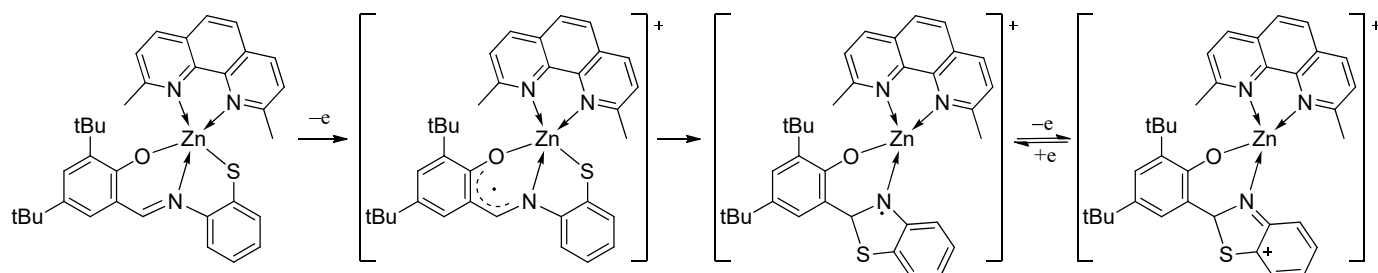


Figure 7. Cyclic voltammograms of **7**: the potential switch from -1.80 to 0.90 V (curve 1); the potential switch from -0.50 to 1.45 V (curve 2) (CH_2Cl_2 , $C = 2$ mmol, 0.1 M TBAP, scan rate 200 $\text{mV}\cdot\text{s}^{-1}$).

This behaviour can be explained by the occurrence of an intramolecular cyclization reaction in the coordination sphere of the metal in **7** with the formation of a heterocyclic radical (Scheme 4).



Scheme 4. Two electrochemical oxidations of **7** with the intramolecular cyclization stage.

Stabilization of this type of intermediate can be achieved due to the presence of a neocuproine ligand in **7**, since complex **6** with the Bipy ligand does not exhibit such behaviour. For Schiff bases acting as ligands, electrically induced cyclization is a typical reaction [44,45]. The ratio of currents for the second stage is less than 1, which implies the occurrence of the subsequent chemical stage, i.e., deprotonation of the tertiary carbon atom with the formation of benzothiazole. Complexes **4** and **5** are characterized by additional anodic steps in the potential range from 1.55 to 1.62 V, which are comparable with the second oxidation potentials (1.56–1.66 V) of free ligands, which may indicate the decoordination of Schiff bases and subsequent reactions deeper oxidation.

2.3.2. Reduction

For complexes **1–3**, several peaks are recorded in the cathodic region in the range from -1.30 to -1.74 V (Figure 8, Figures S20 and S21). In view of the presence of an electroactive NO_2 group, the reduction mechanism of these compounds becomes much more complicated.

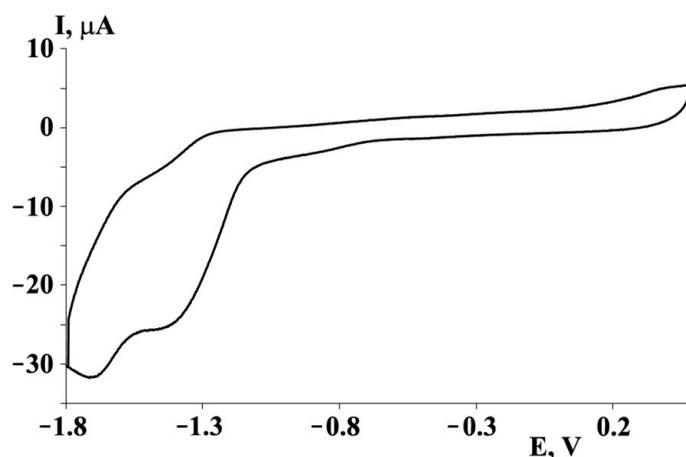


Figure 8. Cyclic voltammogram of **3** the potential switch from 0.50 to -1.80 V (CH_2Cl_2 , $C = 2$ mmol, 0.1 M TBAP, scan rate 200 $\text{mV}\cdot\text{s}^{-1}$).

For compounds **1** and **2**, a weakly resolvable pre-peak at -1.30 V is observed, which presumably corresponds to the reduction of the nitro group. For a free ligand, a similar redox process is also irreversible, but it is observed at a potential of -0.70 V. Taking into account the presence of the dianionic form of the ligand in **1** and **2** and the expected shift of reduction potentials to the cathodic region, it can be assumed that the nitro group is involved in this electrode process. The additional cathode peaks observed in the range of -1.40 to -1.50 V are in good agreement with the previously obtained results for zinc complexes with coordinated bipyridyl or phenanthroline and an additional S-donor ligand [46,47]. The coordination of the azomethine group at the zinc atom also allows us to consider the possibility of its participation in the cathode stage, however, then one would expect fairly close values of the reduction potentials in a series of complexes **1–3**. However, a rather large scatter of potential values is observed. For most other complexes, the first reduction step is quasi-reversible and one-electron (e.g., complexes **8**, **4** and **6**, Figure 9, Figures S23 and S26, respectively).

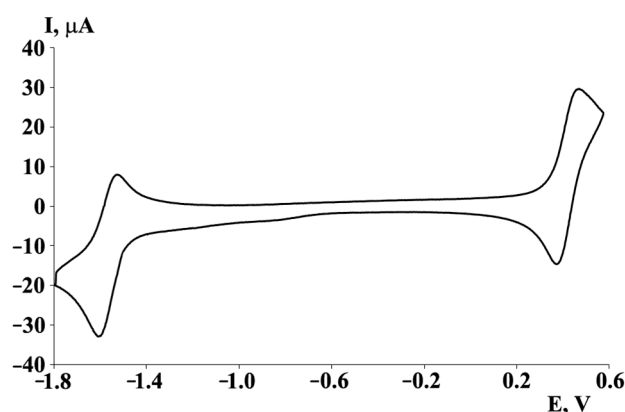
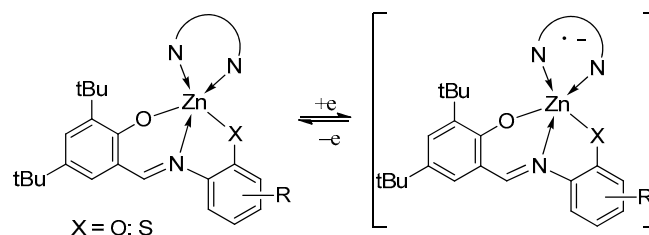


Figure 9. Cyclic voltammogram of **8** the potential switch from 0.55 to -1.80 V (CH_2Cl_2 , $C = 2$ mmol, 0.1 M TBAP, scan rate 200 $\text{mV}\cdot\text{s}^{-1}$).

As a result of the electrochemical reduction stage, a relatively stable monoanionic complex is formed (Scheme 5). Based on the ratios of the currents, the most stable monoanions are generated during the electroreduction of complexes **6–8**.



Scheme 5. The electrochemical formation of monoanionic derivatives.

In the case of complexes **1** and **4**, the proximity of the peak potentials (-1.49 and -1.51 V) indicates the participation of bipyridyl in the cathode stage, while for compounds **6** and **8**, the $E^{\text{red}1}_{1/2}$ values are shifted to the cathodic region (Table 2). The observed regularities suggest the presence of mutual influence of two types of ligands. The sensitivity of the values of the reduction potentials depending on the O,N,O'- or O,N,S-donor ligand is fixed, for example, for complexes **4** and **6**, where the $E^{\text{red}1}_{1/2}$ value for complex **6** is shifted to the cathode region up to -1.56 V.

The nature of the substituents in the redox-active Schiff base influences the values of the oxidation potentials. In the case of **1** and **4**, the replacement of the electron-withdrawing nitro group by a chlorine atom with the simultaneous introduction of a methyl substituent leads to a decrease in the oxidation potential by 0.17 V, as well as the presence of two donor tert-butyl groups in **8**. A more pronounced effect is observed for pairs **2** and **5**, or **1** and **8**, for which there is a synchronous shift of $E^{\text{ox}1}_{1/2}$ and $E^{\text{ox}2}$ to the cathode region. For complexes **1** and **2**, the transition from bipyridyl to phenanthroline ligand does not affect the value of the oxidation potential. At the same time, for complex **3**, this value shifts to the anode region, as well as the reduction potential. This fact indicates the presence of a weak electronic interaction between two redox-active ligands. A distinctive feature of compounds **5** and **8** containing donor tert-butyl groups in the O,N,O'-ligand is the stabilization of the monocationic and monoanionic forms of the complexes. The Schiff base takes part in the electrooxidation, while the neutral nitrogen-containing ligand is involved to a greater extent in the cathodic process. An analysis of the potential values suggests that, on the one hand, these complexes act as electron donors and are easily oxidized, and on the other hand, they are weak electron acceptors. This dual behaviour allows us to consider them as electronic reservoirs, which makes it possible to use this type of complexes to initiate photoinduced redox transformations or as electrocatalysts.

One of the main indicators used to assess the possibility of using substances in photo-voltaic devices is the energy gap (ΔE), which is the difference in the energies of the boundary orbitals. The value of ΔE can be determined theoretically using quantum chemical calculations or measured experimentally using electrochemistry or UV-visible spectroscopy. Electrochemical methods are widely used to determine the electrochemical gap ΔE_{el} since the values of the standard reduction and oxidation potentials correlate with the LUMO and HOMO energies. In the case of most of the studied complexes, this value was determined as the difference in the potentials of the peaks (Table 2). The values of ΔE_{el} range from 1.97 to 2.42 eV, while the minimum values were obtained for complexes 5 and 8. The sequential replacement of electron-withdrawing groups in the Schiff base with donor ones leads to a decrease in the value of ΔE_{el} in a row of 1, 4, 8, or for 2 and 5. This effect is observed mainly due to a decrease in the value of the first oxidation potential due to the involvement of the coordinated Schiff base in the redox processes. In the series of complexes 1–3, the ΔE_{el} parameter is not significantly affected by the auxiliary neutral ligand.

2.4. UV-Vis Spectroscopy and DFT Calculations

According to the literature data, an overestimation of ΔE_{el} compared to the spectral value (ΔE) is typical for polymers and crystalline materials, while the opposite effect is recorded for low molecular weight compounds [48]. As a result, we have studied the activity of the complexes in the UV-visible range of the spectrum (280–600 nm) in chloroform (Table 3). For the investigated zinc(II) complexes in this spectral range, two or three absorption bands are observed with an intensity maximum in the region of 430–500 nm (Table 3, Figure 10).

Table 3. The UV-vis spectral data for 1–8 in CHCl_3 solution at 293 K.

No.	Compound	λ_{Max} , nm (ϵ , $10^3 \text{ M}^{-1}\text{cm}^{-1}$)	ΔE , eV
1	(L ¹)Zn(Bipy)	305 (16.6), 385 (6.5), 490 (18.7)	2.53
2	(L ¹)Zn(Phen)	378 (4.4), 491 (17.1)	2.52
3	(L ¹)Zn(Neo)	385 (4.6), 497 (18.0)	2.49
4	(L ²)Zn(Bipy)	304 (28.5), 376 (10.2), 457 (28.8)	2.71
5	(L ³)Zn(Phen)	310 (6.6), 382 (4.7), 448 (10.8)	2.76
6	(L ⁵)Zn(Bipy)	303 (20.0), 432 (10.1)	2.87
7	(L ⁵)Zn(Neo)	316 (6.9), 438 (10.6)	2.82
8	(L ⁴)Zn(Bipy)	307 (9.8), 381 (9.7), 451 (7.7)	2.74

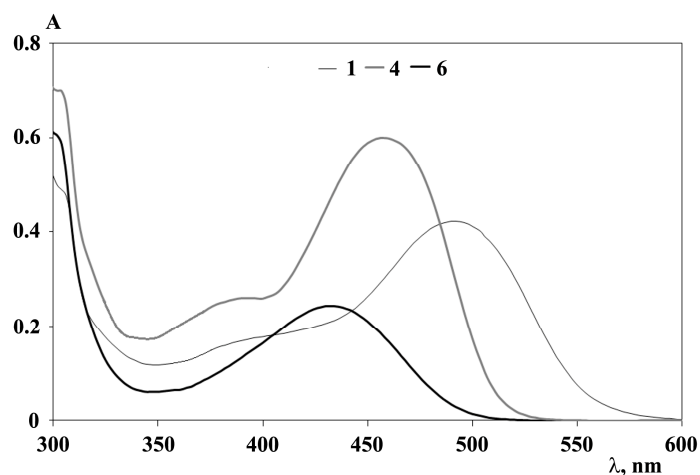


Figure 10. The UV-vis spectra of complexes 1, 4, 6 in CHCl_3 at 293 K ($C = 2.5 \times 10^{-5} \text{ mol/L}$).

The largest shift of the absorption maximum to the long wavelength region is characteristic of complexes 1–3 with an electron-withdrawing nitro group. The introduction of donor substituents into the Schiff base, on the contrary, promotes a hypsochromic shift of λ_{\max} in the visible region of the spectrum for complexes 4, 5, and 8. The replacement of an oxygen atom by sulfur in the case of compounds 6 and 7 has a similar effect on the position of the absorption maximum. The calculated values of the energy gap for the complexes are observed in a narrow range from 2.49 to 2.87 eV. The closer values of ΔE , which are consistent with the results of measuring ΔE_{el} , were obtained only for the first three zinc(II) complexes. In other cases, the ΔE values have higher values than those obtained on the basis of the electrochemical studies.

The density functional theory calculations were performed for molecules 4, 6 and 8 at the PBE0-D3/6-311++G(d,p) level in CHCl_3 solution (the SCRF-PCM model) to unambiguously describe the observed spectral data. Noteworthy, while the geometry optimization led to insignificant changes in the structures of 6 and 8 molecules as compared to those in crystals (rmsd 0.1022 and 0.087 Å, respectively), the resulting structure of 4·H₂O (Figure S28) is characterized by the pentacoordinate metal atom with the water molecule participating only in a moderate hydrogen bond with the oxygen O2 atom (O3 . . . O2 2.722 Å, the O2-H-O3 angle equals to 165.0°). The solution of the time-dependent Kohn-Sham equations for the optimized structures with the accounting of non-equilibrium PCM solvation reasonably describes corresponding spectral data in the long-wave regions. Namely, the excitation energies for the simplest allowed transitions having the largest oscillator strength values do correspond to the λ_{Max} values with a rather good accuracy (452, 425, and 460 nm for 4, 6, and 8, respectively). A closer look at these transitions revealed that neither of them involves the metal atom region. In 4, the transition corresponds to the intraligand excitation from the π -bonding (HOMO) to the π^* orbital (LUMO+1) both centered on the Schiff ligand (Figure 11). Note that the HOMO orbital also covers regions of the lone electronic pairs on chlorine atoms while the LUMO+1 orbital does not; hence, the corresponding transition can be described as the combination of n- π and π - π intraligand charge transfers. For 6 and 8, the interligand charge transfer is observed that corresponds to the excitations from the same HOMO π -bonding orbital of the Schiff base to the LUMO+1 and LUMO+2 π -antibonding orbitals centered on both ligands (Figure 12). The additional calculations for the other complexes under study demonstrated a similar order of molecular orbitals (Figures S29 and S30): for instance, the HOMO is always a π -bonding orbital located on the Schiff base, and the LUMO is located on a neutral NN ligand. This allows to assume that the discussed excitation mechanisms could be a common feature for this class of compounds.

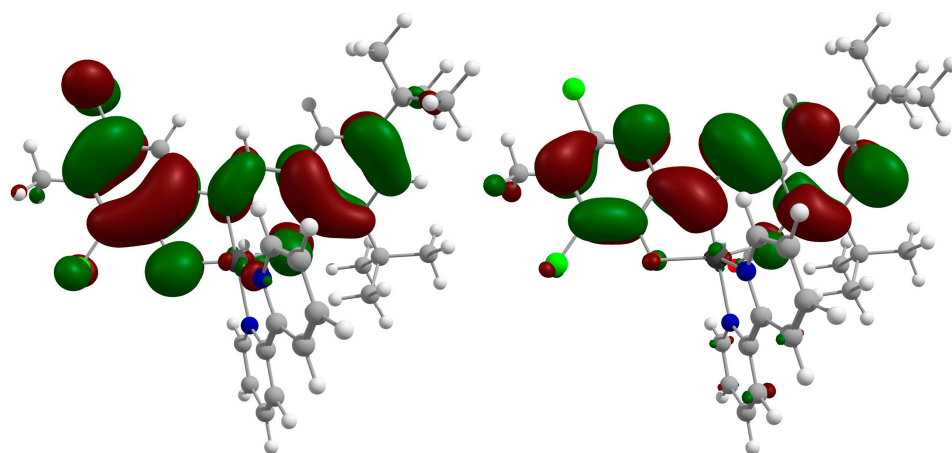


Figure 11. The isosurfaces of HOMO (left) and LUMO+1 (right) in the optimized structure of 4.

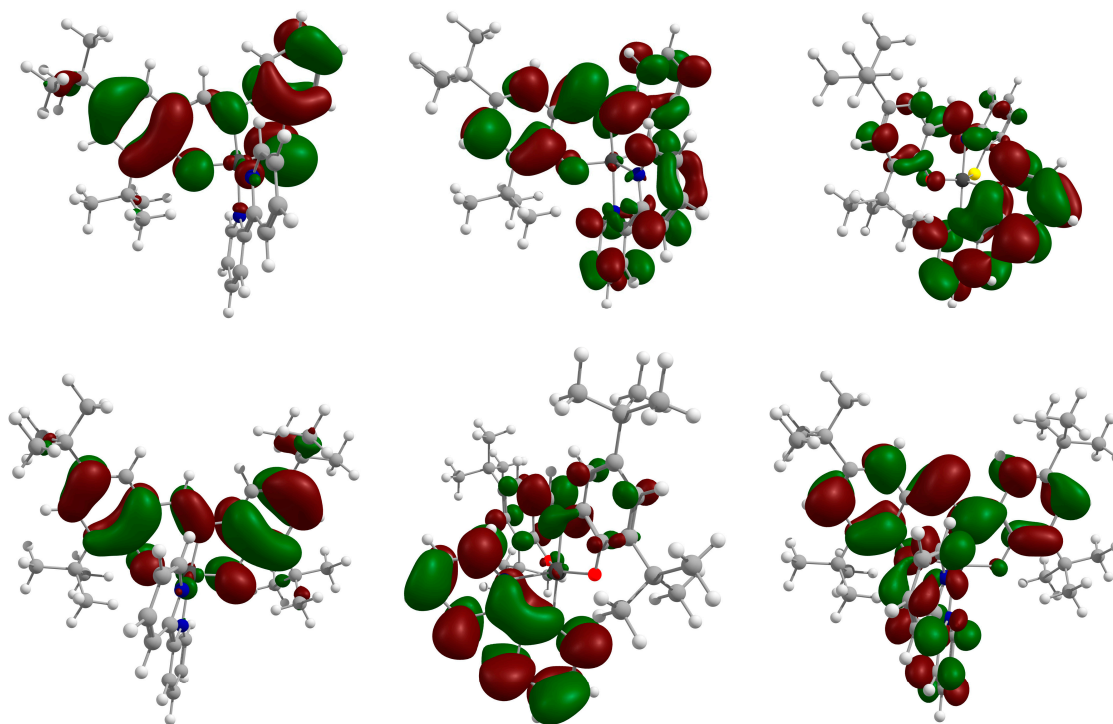


Figure 12. The isosurfaces of HOMO (left), LUMO+1 (middle) and LUMO+2 (right) orbitals for the optimized structures of **6** (top) and **8** (bottom).

3. Materials and Methods

3.1. General

The starting reagents were commercially available ZnCl_2 (anhydrous, «Ekros», 99%, Saint Petersburg, Russia), 3,5-di-*tert*-butylsalicylic aldehyde («Acros Organics», 99%, Shanghai, China), 2-amino-4-*tert*-butylphenol («Alfa Aesar», 97%, Heysham, England), 2-amino-4-chloro-6-nitrophenol («Aldrich», 97%, Burlington, MA, USA), 6-amino-2,4-dichloro-3-methylphenol hydrochloride (Fluka, 97%, Steinheim, Germany), 2-aminothiophenol ($\geq 97\%$, Hohenbrunn, Germany), 2,2'-bipyridine (98%, Sigma Aldrich, Saint Louis, MO, USA), 1,10-phenanthroline (99%, Alfa Aesar, Shanghai, China), neocuproine hemihydrate (99+%, Acros Organics, Waltham, MA, USA) tetrabutylammonium perchlorate (Bu_4NClO_4) («Alfa Aesar», 99%, China) were used without further purification. 4,6-Di-*tert*-butyl-*o*-aminophenol was synthesized by the known method [49]. Solvents were purified following standard procedures [50].

The IR spectra were recorded on an FSM-1201 FT-IR spectrometer (LLC «Monitoring», Saint Petersburg, Russia) in KBr pellets. The NMR spectra were measured in CDCl_3 on Bruker Avance HD 400 spectrometers (Bruker Biospin AG, Faellanden, Switzerland) with a frequency of 400 MHz (^1H) and 100 MHz (^{13}C) using Me_4Si as an internal standard. The chemical shift values are given in ppm with reference to the solvent, and the coupling constants (J) are given in Hz. The elemental analysis was carried out on a Euro EA 3000 (C,H,N) elemental analyzer (EuroVector Srl, Redavalle, Italy). Mass spectra (HRMS) were recorded on a Bruker UHR-TOF MaxisTM Impact mass spectrometer (Bruker Daltonik GmbH, Bremen, Germany). The UV-VIS spectra were recorded with a SF-104 spectrophotometer (AKVILON, Podol'sk, Russia) in a range of 300–600 nm.

3.2. Synthesis and Characterization

3.2.1. General Method for Preparation of Tridentate Schiff Bases

Reactions of 3,5-di-*tert*-butyl-2-hydroxybenzaldehyde (4 mmol) with *o*-aminophenols or *o*-aminothiophenols (4 mmol) were carried out in methanol (20 mL). The appropriate aminothiophenol (in 1 mL methanol) was added dropwise to a solution of aldehyde (in 20 mL) for 30 min, and then the solution was refluxed for 5 h under argon. The solution was

slowly cooled to room temperature. The resulting precipitate was filtered off and dried under reduced pressure. The Schiff bases such as 2-(*E*)-(2-Mercaptophenylimino)methyl)-4,6-di-*tert*-butylphenol (L^5H_2), 2,4-di-*tert*-butyl-6-(((5-*tert*-butyl)-2-hydroxyphenyl)imino)methyl)phenol (L^3H_2) were synthesized by the known methods [21,51].

3.2.2. L^1H_2

Yield 1.14 g, 2.8 mmol (62%). IR (KBr, ν/cm^{-1}): 3225, 3082, 2961, 2910, 2870, 1620, 1597, 1580, 1522, 1470, 1435, 1408, 1363, 1310, 1248, 1202. 1H NMR (400 MHz, $CDCl_3$, δ , ppm): 1.33 (s, 9H, tBu), 1.48 (s, 9H, tBu), 7.24 (d, $^4J(H,H) = 2.4$ Hz, 1H, arom. C_6H_2), 7.47 (d, $^4J(H,H) = 2.5$ Hz, 1H, arom. C_6H_2), 7.52 (d, $^4J(H,H) = 2.4$ Hz, 1H, arom. C_6H_2), 8.01 (d, $^4J(H,H) = 2.5$ Hz, 1H, arom. C_6H_2), 8.74 (s, 1H, CH=N), 10.87 (s, 1H, OH), 13.24 (br.s, 1H, OH). ^{13}C $\{^1H\}$ NMR (100 MHz, $CDCl_3$, δ , ppm): 29.38, 31.39, 34.20, 35.16, 117.90, 121.24, 124.88, 127.18, 127.26, 129.51, 134.25, 137.48, 140.83, 140.99, 148.11, 158.86, 166.65. Calcd. for $C_{21}H_{25}ClN_2O_4$ (%): C, 62.30; H, 6.22; N, 6.92. Found (%): C, 62.18; H, 6.47; N, 7.01.

3.2.3. L^2H_2

Yield 1.14 g, 2.8 mmol (70%). IR (KBr, ν/cm^{-1}): 3515, 3532, 3008, 2961, 2910, 2869, 1613, 1580, 1470, 1434, 1395, 1373, 1361, 1334, 1295, 1273, 1251, 1229, 1202. 1H NMR (400 MHz, $CDCl_3$, δ , ppm): 1.33 (s, 9H, tBu), 1.47 (s, 9H, tBu), 2.48 (s, 3H, CH_3), 5.97 (br.s, 1H, OH), 7.17 (s, 1H, arom. C_6H_1), 7.24 (d, $^4J(H,H) = 2.4$ Hz, 1H, arom. C_6H_2), 7.49 (d, $^4J(H,H) = 2.4$ Hz, 1H, arom. C_6H_2), 8.70 (s, 1H, CH=N), 12.93 (br.s, 1H, OH). ^{13}C $\{^1H\}$ NMR (100 MHz, $CDCl_3$, δ , ppm): 17.69, 29.39, 31.41, 34.21, 35.12, 117.86, 118.18, 121.96, 125.95, 127.26, 129.03, 132.95, 134.62, 137.24, 141.08, 144.61, 158.21, 165.50. EI-MS: Found m/z : 408.1498 $[M + H]^+$. $C_{22}H_{28}Cl_2NO_2$. Calcd m/z : 408.1492.

3.2.4. L^4H_2

Yield 1.10 g, 2.5 mmol (62%). IR (KBr, ν/cm^{-1}): 3519, 3458, 2957, 2907, 2866, 1615, 1584, 1481, 1468, 1440, 1413, 1392, 1361, 1331, 1271, 1250, 1219, 1200. 1H NMR (400 MHz, $CDCl_3$, δ , ppm): 1.35 (s, 9 H, tBu), 1.36 (s, 9 H, tBu), 1.46 (s, 9 H, tBu), 1.48 (s, 9 H, tBu), 6.23 (br.s, 1 H, OH), 7.02 (d, $^4J(H,H) = 2.1$ Hz, 1 H, arom. C_6H_2), 7.28 (d, $^4J(H,H) = 2.1$ Hz, 1 H, arom. C_6H_2), 7.30 (d, $^4J(H,H) = 2.3$ Hz, 1 H, arom. C_6H_2), 7.50 (d, $^4J(H,H) = 2.3$ Hz, 1 H, arom. C_6H_2), 8.70 (s, 1 H, CH=N), 12.69 (br.s, 1 H, OH). ^{13}C $\{^1H\}$ NMR (100 MHz, $CDCl_3$, δ , ppm): 29.40, 29.50, 31.45, 31.62, 34.25, 34.59, 35.05, 35.71, 112.66, 118.63, 123.01, 127.27, 128.70, 135.39, 135.77, 137.25, 141.30, 142.47, 146.12, 157.55, 164.63. EI-MS: Found m/z : 438.3358 $[M + H]^+$. $C_{29}H_{44}NO_2$. Calcd m/z : 438.3367.

3.2.5. General Method for Preparation of Zinc Complexes 1–8

Synthesis of zinc complexes was carried out as follows: 1 equiv. neutral nitrogen-containing ligand (NN) (0.35 mmol) dissolved in acetonitrile (2 mL) was added to a solution of $ZnCl_2$ (0.35 mmol) in the same solvent (5 mL) under argon. As a result of mixing, a suspension of the (NN) $ZnCl_2$ complex is formed, then 0.35 mmol of Schiff base and 2 equiv. triethylamine (0.7 mmol) were added under extensive stirring. During the reaction, the initial precipitate of (NN) $ZnCl_2$ gradually dissolved and the color of the solution changed to intense orange or brick red. The resulting solution was left for 2 days at 0–4 °C. The resulting colored precipitates of the complexes were filtered off, washed with *n*-hexane, and dried under reduced pressure. Crystals suitable for X-ray diffraction analysis were obtained by recrystallization of the compounds in acetonitrile.

3.2.6. (L^1)Zn(Bipy) (1) O,N,O'-(2,4-Di-*tert*-butyl-6-((5-chloro-3-nitro-2-oxidophenylimino)methyl)phenolato)-N,N'-(2,2'-bipyridyl)zinc(II)

The yield of **1** in the form of red crystals was 43% (0.094 g). IR (KBr, cm^{-1}): 3076, 2954, 2903, 2869, 1600, 1543, 1522, 1507, 1473, 1458, 1442, 1385, 1340, 1252, 1215, 1200, 1160, 1131, 1103. 1H NMR (400 MHz, $CDCl_3$, δ/J , ppm/Hz): 0.98 (s, 9H, tBu), 1.28 (s, 9H, tBu),

7.00 (s, 1H, arom. C₆H₂), 7.26 (s, 1H, arom. C₆H₂), 7.46 (br.t, J = 5.9 Hz, 2 H, 2,2'-bipy), 7.55 (s, 1H, arom. C₆H₂), 7.72 (s, 1H, arom. C₆H₂), 7.98 (br.t, J = 6.8 Hz, 2 H, 2,2'-bipy), 8.18 (br.d, J = 5.9 Hz, 2 H, 2,2'-bipy), 8.58 (br.s, 2 H, 2,2'-bipy), 8.67 (s, 1H, CH=N). ¹³C NMR (100 MHz, CDCl₃, δ, ppm): 28.88, 31.27, 33.83, 35.03, 115.97, 117.89, 118.26, 121.43, 121.45, 123.08, 126.59, 128.59, 129.62, 134.87, 137.93, 140.25, 140.30, 141.27, 141.51, 149.06, 161.68. Calcd. for C₃₁H₃₁ClN₄O₄Zn (%): C, 59.63; H, 5.00; N, 8.97. Found (%): C, 59.84; H, 5.25; N, 8.92.

3.2.7. (L¹)Zn(Phen) (2) O,N,O'-(2,4-Di-tert-butyl-6-((5-chloro-3-nitro-2-oxidophenylimino)methyl)phenolato)-N,N'-(1,10-phenanthroline)zinc(II)

The yield of **2** in the form of red powder was 65% (0.147 g). IR (KBr, cm⁻¹): 3079, 3059, 2954, 2903, 2873, 1597, 1544, 1519, 1458, 1429, 1407, 1386, 1337, 1253, 1198, 1156, 1104. ¹H NMR (400 MHz, CDCl₃, δ/J, ppm/Hz): 0.81 (s, 9H, tBu), 1.28 (s, 9H, tBu), 6.96 (d, J = 2.5 Hz, 1H, arom. C₆H₂), 7.20 (d, J = 2.5 Hz, 1H, arom. C₆H₂), 7.57 (d, J = 2.6 Hz, 1 H, arom. C₆H₂), 7.62-7.68 (m, 3H: 1H, arom. C₆H₂ + 2H, Phen), 7.94 (s, 2H, Phen), 8.43 (d, J = 8.0 Hz, 2 H, Phen), 8.66 (s, 1 H, CH=N), 8.86 (d, J = 3.9 Hz, 2 H, Phen). ¹³C NMR (100 MHz, CDCl₃, δ, ppm): 28.72, 31.24, 33.80, 34.89, 116.31, 117.80, 118.27, 122.89, 124.79, 126.83, 128.46, 128.75, 129.51, 134.53, 138.09, 138.68, 141.12, 142.07, 149.10, 157.75, 161.39, 170.91. EI-MS: Found *m/z*: 647.1353 [M + H]⁺. C₃₃H₃₂ClN₄O₄Zn. Calcd. *m/z*: 647.1398.

3.2.8. (L¹)Zn(Neo) O,N,O'-(2,4-Di-tert-butyl-6-((5-chloro-3-nitro-2-oxidophenylimino)methyl)phenolato)-N,N'-(2,9-dimethyl-1,10-phenanthroline)zinc(II)

The yield of **3** in the form of red crystals was 46% (0.109 g). IR (KBr, cm⁻¹): 3070, 2955, 2903, 2867, 1594, 1572, 1542, 1522, 1507, 1460, 1426, 1410, 1361, 1340, 1255, 1210, 1197, 1160, 1131, 1104. ¹H NMR (400 MHz, CDCl₃, δ/J, ppm/Hz): 0.62 (s, 9H, tBu), 1.27 (s, 9H, tBu), 2.76 (s, 6H, CH₃, Neo), 3.18 (s, 3H, CH₃, free 1/2Neo), 7.05 (d, J = 2.3 Hz, 1H, arom. C₆H₂), 7.20 (d, J = 2.3 Hz, 1H, arom. C₆H₂), 7.57 (d, J = 8.3 Hz, 2 H, arom., Neo), 7.62 (d, J = 2.6 Hz, 1H, arom. C₆H₂), 7.77 (dd, J = 8.3 Hz, J = 0.8 Hz, 1H, arom., free 1/2Neo), 7.84 (d, J = 0.8 Hz, 2H, arom., Neo), 7.85 (d, J = 2.6 Hz, 1H, arom. C₆H₂), 7.91 (d, J = 0.8 Hz, 1H, arom., free 1/2Neo), 8.36 (dd, J = 8.3 Hz, J = 0.8 Hz, 2 H, arom., Neo), 8.47 (dd, J = 8.3 Hz, J = 0.8 Hz, 1H, arom., free 1/2Neo), 8.82 (s, 1 H, CH=N). ¹³C NMR (100 MHz, CDCl₃, δ, ppm): 25.00, 25.02, 28.39, 31.26, 33.83, 34.63, 115.32, 117.47, 118.01, 122.91, 125.50, 125.75, 125.95, 126.41, 127.00, 127.09, 128.69, 129.57, 134.61, 137.57, 138.98, 139.87, 140.16, 140.74, 140.77, 141.18, 158.73, 158.98, 160.68, 161.30, 171.32. Calcd. for C₄₂H₄₁ClN₅O₄Zn ((L¹)Zn(Neo)-0.5Neo) (%): C, 64.62; H, 5.29; N, 8.97. Found (%): C, 64.90; H, 5.49; N, 8.78.

3.2.9. (L²)Zn(Bipy) (4) O,N,O'-(2,4-Di-tert-butyl-6-((3,5-dichloro-4-methyl-2-oxidophenylimino)methyl)phenolato)-N,N'-(2,2'-bipyridyl)zinc(II)

The yield of **4** in the form of bright orange crystals was 47% (0.110 g). IR (KBr, cm⁻¹): 3076, 2951, 2907, 2870, 1605, 1587, 1520, 1458, 1447, 1407, 1383, 1361, 1316, 1253, 1228, 1196, 1157, 1139. ¹H NMR (400 MHz, CDCl₃, δ/J, ppm/Hz): 0.96 (s, 9H, tBu), 1.28 (s, 9H, tBu), 2.38 (s, 3H, CH₃), 7.01 (d, J = 2.4 Hz, 1H, arom. C₆H₂), 7.21 (d, J = 2.4 Hz, 1H, arom. C₆H₂), 7.36-7.45 (m, 3 H: 2H, 2,2'-bipy + 1H, arom. C₆H₁), 7.90 (td, J = 7.8 Hz, J = 1.0 Hz, 2H, 2,2'-bipy), 8.16 (d, J = 7.9 Hz, 2H, 2,2'-bipy), 8.59 (d, J = 4.6 Hz, 2 H, 2,2'-bipy), 8.69 (s, 1H, CH=N). ¹³C NMR (100 MHz, CDCl₃, δ, ppm): 18.01, 28.95, 31.39, 33.78, 34.97, 105.73, 112.32, 118.34, 121.43, 125.86, 128.31, 132.18, 134.10, 134.59, 139.75, 139.80, 140.70, 149.03, 149.07, 159.61, 169.73. Calcd. for C₃₂H₃₃Cl₂N₃O₂Zn (%): C, 61.21; H, 5.30; N, 6.69. Found (%): C, 61.48; H, 5.46; N, 6.51.

3.2.10. (L³)Zn(Phen) (5) O,N,O'-(2,4-Di-tert-butyl-6-((5-tert-butyl-2-oxidophenylimino)methyl)phenolato)-N,N'-(1,10-phenanthroline)zinc(II)

The yield of **5** in the form of orange powder was 68% (0.165 g). IR (KBr, cm⁻¹): 3050, 2951, 2902, 2866, 1609, 1593, 1539, 1520, 1486, 1458, 1428, 1382, 1362, 1300, 1273, 1253, 1230, 1196, 1160, 1141, 1127, 1102. ¹H NMR (400 MHz, CDCl₃, δ/J, ppm/Hz): 0.81 (s, 9H, tBu), 1.29 (s, 9H, tBu), 1.38 (s, 9H, tBu), 6.78 (d, J = 8.4 Hz, 1H, arom. C₆H₃), 7.03 (dd, J = 8.4 Hz, J = 1.7 Hz, 1H, arom. C₆H₃), 7.10 (d, J = 2.3 Hz, 1 H, arom. C₆H₂), 7.15 (d, J = 2.3 Hz, 1 H, arom. C₆H₂), 7.56 (d, J = 1.7 Hz, 1 H, arom. C₆H₃), 7.68 (m, 2H, Phen), 7.89 (s, 2H, Phen), 8.38 (d, J = 7.8 Hz, 2 H, Phen), 8.84 (s, 1 H, CH=N), 8.94 (d, J = 3.7 Hz, 2 H, Phen). ¹³C NMR (100 MHz, CDCl₃, δ, ppm): 28.72, 31.52, 31.88, 33.80, 34.14, 34.84, 108.98, 118.39, 118.92, 124.68, 125.14, 126.66, 127.25, 128.38, 128.65, 133.49, 134.23, 136.25, 138.12, 140.37, 141.33, 149.22, 157.88, 159.44, 168.60. EI-MS: Found *m/z*: 624.2575 [M + H]⁺. C₃₇H₄₂N₃O₂Zn. Calcd. *m/z*: 624.2563.

3.2.11. (L⁵)Zn(Bipy) (6) O,N,S-(2,4-Di-tert-butyl-6-((2-sulfidophenylimino)methyl)phenolato)-N,N'-(2,2'-bipyridyl)zinc(II)

The yield of **6** in the form of orange crystals was 35% (0.069 g). IR (KBr, cm⁻¹): 3066, 3042, 2954, 2904, 2867, 1603, 1574, 1524, 1490, 1475, 1458, 1439, 1382, 1360, 1330, 1313, 1273, 1251, 1236, 1157, 1135, 1101. ¹H NMR (400 MHz, CDCl₃, δ/J, ppm/Hz): 1.04 (s, 9H, tBu), 1.28 (s, 9H, tBu), 6.96–7.07 (m, 2H, arom., C₆H₄), 7.04 (d, J = 2.4 Hz, 1H, arom. C₆H₂), 7.25 (d, J = 2.4 Hz, 1H, arom. C₆H₂), 7.41–7.47 (m, 3 H: 2H, 2,2'-bipy + 1H, arom. C₆H₄), 7.60 (dd, J = 7.2 Hz, J = 1.8 Hz, 1 H, arom. C₆H₄), 7.92 (td, J = 7.8 Hz, J = 1.8 Hz, 2H, arom. 2,2'-bipy), 8.10 (d, J = 8.0 Hz, 2 H, 2,2'-bipy), 8.54 (d, J = 4.4 Hz, 2 H, 2,2'-bipy), 8.63 (s, 1H, CH=N). ¹³C NMR (100 MHz, CDCl₃, δ, ppm): 28.94, 31.41, 33.76, 35.01, 115.34, 118.51, 121.11, 122.54, 125.91, 126.20, 128.62, 128.85, 133.27, 134.06, 139.53, 140.78, 146.52, 148.77, 149.00, 163.83, 168.65. Calcd. for C₃₁H₃₃N₃OSZn (%): C, 66.36; H, 5.93; N, 7.49. Found (%): C, 66.21; H, 6.12; N, 7.39.

3.2.12. (L⁵)Zn(Neo) (7) O,N,S-(2,4-Di-tert-butyl-6-((2-sulfidophenylimino)methyl)phenolato)-N,N'-(2,9-dimethyl-1,10-phenanthroline)zinc(II)

The yield of **7** in the form of light orange powder was 41% (0.069 g). IR (KBr, cm⁻¹): 3048, 2952, 2904, 2866, 1598, 1575, 1522, 1508, 1460, 1426, 1381, 1364, 1332, 1272, 1252, 1235, 1200, 1159, 1138, 1102. ¹H NMR (400 MHz, CDCl₃, δ/J, ppm/Hz): 0.69 (s, 9H, tBu), 1.28 (s, 9H, tBu), 2.85 (s, 6H, CH₃, Neo), 7.00–7.04 (m, 2H, arom., C₆H₄), 7.07 (d, J = 2.6 Hz, 1H, arom. C₆H₂), 7.21 (d, J = 2.6 Hz, 1H, arom. C₆H₂), 7.38–7.44 (m, 1H, arom., C₆H₄), 7.54 (d, J = 8.3 Hz, 2 H, arom., Neo), 7.61–7.68 (m, 1H, arom., C₆H₄), 7.81 (s, 2H, arom., Neo), 8.28 (d, J = 8.3 Hz, 2 H, arom., Neo), 8.71 (s, 1 H, CH=N). ¹³C NMR (100 MHz, CDCl₃, δ, ppm): 24.94, 28.55, 31.41, 33.77, 34.57, 116.18, 118.20, 122.37, 125.59, 125.65, 125.90, 127.08, 128.44, 128.87, 132.95, 133.77, 138.14, 140.53, 141.04, 142.75, 146.20, 159.41, 163.65, 169.57. Calcd. for C₃₅H₃₇N₃OSZn (%): C, 68.56; H, 6.08; N, 6.85. Found (%): C, 68.63; H, 6.27; N, 6.79.

3.2.13. (L⁴)Zn(Bipy) (8) O,N,O'-(2,4-Di-tert-butyl-6-((3,5-di-tert-butyl-2-oxidophenylimino)methyl)phenolato)-N,N'-(2,2'-bipyridyl)zinc(II)

The yield of complex in the form of red crystals was 30% (0.069 g). IR (KBr, cm⁻¹): 3103, 3069, 2951, 2907, 2870, 1607, 1598, 1578, 1560, 1542, 1522, 1475, 1443, 1409, 1377, 1315, 1297, 1275, 1253, 1230, 1198, 1161. ¹H NMR (400 MHz, CDCl₃, δ/J, ppm/Hz): 1.04 (s, 9H, tBu), 1.23 (s, 9H, tBu), 1.31 (s, 9H, tBu), 1.37 (s, 9H, tBu), 7.09 (d, J = 2.4 Hz, 1H, arom. C₆H₂), 7.11 (d, J = 2.7 Hz, 1H, arom. C₆H₂), 7.19 (d, J = 2.7 Hz, 1 H, arom. C₆H₂), 7.19 (d, J = 2.4 Hz, 1 H, arom. C₆H₂), 7.48–7.52 (m, 2 H, 2,2'-bipy), 8.01 (t, J = 7.5 Hz, 2H, 2,2'-bipy), 8.13 (d, J = 7.9 Hz, 2H, 2,2'-bipy), 8.65 (d, J = 4.3 Hz, 2 H, 2,2'-bipy), 8.75 (s, 1H, CH=N). Calcd. for C₃₉H₄₉N₃O₂Zn (%): C, 71.27; H, 7.52; N, 6.39. Found (%): C, 71.47; H, 7.68; N, 6.23.

3.3. X-ray Diffraction

The X-ray diffraction data were collected on a D8 Venture automatic diffractometer using graphite monochromated MoK α (λ 0.71073 Å) radiation. SADABS program [52] was used to perform absorption correction. All structures were solved by direct methods and refined by full-matrix least-squares using the *SHELXL2018/3* [53] with OLEX2 [54]. All the non-hydrogen atoms were refined with anisotropic atomic displacement parameters. The positions of hydrogen atoms were located from the Fourier electron density synthesis and were included in the refinement in the isotropic riding model approximation. The main crystallographic data and structure refinement details for all complexes are presented in Table S2. CCDC 2209787 (**4**·H₂O·CH₃CN), 2209788 (**6**), 2212742 (**8**·CH₃CN) contain the supplementary crystallographic data. These data can also be obtained free of charge at ccdc.cam.ac.uk/structures/ from the Cambridge Crystallographic Data Centre.

3.4. Cyclic Voltammetry

Electrochemical studies were carried out using VERSASTAT-3 potentiostat (PAR) in three-electrode mode. The stationary glassy carbon ($d = 2$ mm) disk was used as the working electrode; the auxiliary electrode was the platinum-flag electrode. The reference electrode was Ag/AgCl/KCl (sat.) with a watertight diaphragm. All measurements were carried out under argon. The samples were dissolved in the pre-deaerated solvent. The scan rate (ν) was 200 mV·s⁻¹. The supporting electrolyte 0.1 M Bu₄NClO₄ was dried under reduced pressure (48 h) at 50 °C. The concentration of compounds was 1–3 mmol.

3.5. Computational Details

The density functional theory calculations were performed using the Gaussian09 program [55]. The PBE0 functional [56,57] and the standard 6-311++G(d,p) basis set was utilized to perform all the calculations. The non-specific solvation effects which can affect molecular properties in a solution were accounted for by means of the SCRF-PCM model [58] ($\epsilon = 4.806$ for CHCl₃). The empirical dispersion correction by Grimme [59] with the Becke-Johnson damping scheme [60] were employed for the geometry optimization procedures. The TD-DFT calculations were performed using the first ten singlet states and including SCRF equilibrium correction.

4. Conclusions

The interaction of O,N,O-, O,N,S-donor Schiff bases derived from 3,5-di-tert-butyl-2-hydroxybenzaldehyde with ZnCl₂ and N,N'-diimine ligands leads to the formation of heteroligand zinc(II) complexes with a preparative yield of up to 68%. The molecular structures of compounds **4**·H₂O, **6**, and **8** in crystal were studied by X-ray diffraction. The data of X-ray diffraction analysis confirm the fact that the Schiff bases in zinc complexes are in the dianionic imino-bis-phenolate or thiophenolate-iminophenolate forms. It is worth noting that the tridentate ligands in the pentacoordinate complexes **6** and **8** are distorted more significantly as compared with the hexacoordinate complex **4**·H₂O.

Due to the redox inertness of the zinc(II) ion, the synthesized complexes are convenient objects for studying the electrochemical behavior, since the contribution of different types of ligands to redox transformations can be estimated. Based on the results of CV experiments, complexes **1**–**3** with electron-withdrawing groups in the O,N,O'-donor ligand tend to form relatively stable monocationic complexes containing oxidized forms of Schiff bases. In the cathodic area for these compounds, the reduction proceeds in irreversible manner and involves both the redox-active nitro-group and the neutral N,N'-donor ligand. The replacement of an oxygen atom by sulfur in complexes **6** and **7** or the introduction of chlorine substituents into the aromatic ring of O,N,O'-redox-active ligand in the case of compound **4** contributes to the destabilization of the electrogenerated oxidized forms. The reversibility of the second oxidation stage for complex **7** can be explained by the intramolecular cyclization reaction with the formation of a heterocyclic radical coordinated at the zinc atom.

Compounds 4–8 are characterized by the participation of neutral N,N' -diimine ligands in redox transformations with the formation of stable monoanion species upon electroreduction. A general tendency for the heteroligand zinc complexes is the separation of ligand functions: in the anodic region, coordinated Schiff bases are predominantly involved in redox processes, while in the cathodic region, neutral N,N' -diimine ligands are participated. A specific feature of compounds 5 and 8 is the possibility to form the relatively stable monoanions and monoanions, which makes it possible to consider these objects as potential reservoirs for electron storage and transfer. Variation in the substituents nature in the Schiff bases affects the oxidation potentials and, accordingly, the reducing activity of this type of complexes. On the one hand, the above complexes are electron donors and are easily oxidized, and on the other hand, they act as weak electron acceptors. This dual behavior causes the use of this type complex to initiate photoinduced redox transformations or as electrocatalysts.

It was found that the variation of the substituents nature in the Schiff base has the greatest effect on the value of ΔE_{el} than the size of the N,N' -diimine aromatic system. The ΔE_{el} values range from 1.97 to 2.42 eV. The minimum values were obtained for complexes 5 and 8 capable of forming stable oxidized/reduced forms. The substitution of electron-withdrawing groups by donor ones in the redox-active ligand promotes a decrease in the first oxidation potential for compounds 4, 5, and 8 and, consequently ΔE_{el} is lowered to 1.97 eV. The calculated values of the energy gap ΔE , determined on the basis of spectral data, are characterized by slightly overestimated values (2.49–2.87 eV) compared to the values of ΔE_{el} , which is typical of low molecular weight compounds.

Supplementary Materials: The following supporting information can be downloaded at: <https://www.mdpi.com/article/10.3390/molecules27238216/s1>, Figures S1–S15 with NMR data; Figures S16–S18 with crystal packing of 4·H₂O·CH₃CN, 6, and 8·CH₃CN; Figures S19–S27 with CV curves for complexes; Figures S28–S30 with DFT results (General view of the optimized molecular structure of 4·H₂O; The isosurfaces of HOMO and LUMO orbitals in the selected complexes); Table S1 with H-bonds in crystals of investigated compounds; Table S2 with the main crystallographic data and structure refinement details.

Author Contributions: Conceptualization, I.V.S. and N.T.B.; methodology, I.V.S., A.I.P.; synthesis, I.V.S., D.A.B.; formal analysis, NMR investigations, A.I.P.; formal analysis, IR spectroscopy, UV-vis spectroscopy, elemental analysis, mass-spectrometry, D.A.B., N.P.P., V.A.F.; cyclic voltammetry, I.V.S., D.A.B.; X-ray diffraction, J.K.V., I.L.E.; theoretical calculations, E.D.T., I.V.A.; investigation, I.V.S., D.A.B., Y.K.V., N.P.P., V.A.F., E.D.T., I.V.A. and I.L.E.; resources, N.T.B.; writing—original draft preparation, A.I.P., I.V.S.; writing—review and editing, A.I.P., I.V.S.; supervision, project administration, I.V.S.; funding acquisition, I.V.S., N.T.B. All authors have read and agreed to the published version of the manuscript.

Funding: This research was funded by Russian Science Foundation, grant number 22-13-00118.

Institutional Review Board Statement: Not applicable.

Informed Consent Statement: Not applicable.

Data Availability Statement: The data presented in this study are available in this article.

Acknowledgments: I.V. Ananyev acknowledges the support of theoretical part (DFT calculations) of this work by the Ministry of Science and Higher Education of the Russian Federation as part of the State Assignment of the Kurnakov Institute of General and Inorganic Chemistry of the Russian Academy of Sciences. The NMR spectroscopic investigations of compounds were carried out in the accordance with State assignment of IOMC RAS using the equipment of the center for collective use “Analytical Center of the IOMC RAS” with the financial support of the grant “Ensuring the development of the material and technical infrastructure of the centers for collective use of scientific equipment” (Unique identifier RF–2296.61321X0017, Agreement Number 075-15-2021-670).

Conflicts of Interest: The authors declare no conflict of interest. The funders had no role in the design of the study; in the collection, analyses, or interpretation of data; in the writing of the manuscript; or in the decision to publish the results.

Sample Availability: Samples of the compounds are available from the authors.

References

1. Tsai, M.-J.; Su, Y.-T.; Wu, J.-Y. Anion Effect on the Formation of Zinc-Salicyaldimine Compounds in Neutral and Anionic Complex Forms: Synthesis, Characterization, ^1H NMR Studies, and Photophysical Properties. *Eur. J. Inorg. Chem.* **2021**, *2021*, 3139–3147. [[CrossRef](#)]
2. Kumar, N.; Roopa; Bhalla, V.; Kumar, M. Beyond zinc coordination: Bioimaging applications of Zn(II)-complexes. *Coord. Chem. Rev.* **2021**, *427*, 213550. [[CrossRef](#)]
3. Abu-Dief, A.M.; El-Sagher, H.M.; Shehata, M.R. Fabrication, spectroscopic characterization, calf thymus DNA binding investigation, antioxidant and anticancer activities of some antibiotic azomethine Cu(II), Pd(II), Zn(II) and Cr(III) complexes. *Appl. Organometal. Chem.* **2019**, *33*, e4943. [[CrossRef](#)]
4. Abu-Dief, A.M.; El-Metwaly, N.M.; Alzahrani, S.O.; Bawazeer, A.M.; Shaaban, S.; Adam, M.S.S. Targeting ctDNA binding and elaborated in-vitro assessments concerning novel Schiff base complexes: Synthesis, characterization, DFT and detailed in-silico confirmation. *J. Mol. Liq.* **2021**, *322*, 114977. [[CrossRef](#)]
5. Pellei, M.; Del Bello, F.; Porchia, M.; Santini, C. Zinc coordination complexes as anticancer agents. *Coord. Chem. Rev.* **2021**, *445*, 214088. [[CrossRef](#)]
6. Zafar, W.; Sumrra, S.H.; Chohan, Z.H. A review: Pharmacological aspects of metal based 1,2,4-triazole derived Schiff bases. *Eur. J. Med. Chem.* **2021**, *222*, 113602. [[CrossRef](#)]
7. Liguori, P.F.; Valentini, A.; Palma, M.; Bellusci, A.; Bernardini, S.; Ghedini, M.; Panno, M.L.; Pettinari, C.; Marchetti, F.; Crispini, A.; et al. Non-classical anticancer agents: Synthesis and biological evaluation of zinc(II) heteroleptic complexes. *Dalton Trans.* **2010**, *39*, 4205–4212. [[CrossRef](#)]
8. Mendiguchia, B.S.; Pucci, D.; Mastropietro, T.F.; Ghedinia, M.; Crispini, A. Non-classical anticancer agents: On the way to water soluble zinc(ii) heteroleptic complexes. *Dalton Trans.* **2013**, *42*, 6768–6774. [[CrossRef](#)]
9. Halevas, E.; Mavroidi, B.; Pelecanou, M.; Hatzidimitriou, A.G. Structurally characterized zinc complexes of flavonoids chrysin and quercetin with antioxidant potential. *Inorg. Chim. Acta* **2021**, *523*, 120407. [[CrossRef](#)]
10. Matos, C.P.; Addis, Y.; Nunes, P.; Barroso, S.; Alho, I.; Martins, M.; Matos, A.P.A.; Marques, F.; Cavaco, I.; Pessoa, J.C.; et al. Exploring the cytotoxic activity of new phenanthroline salicylaldimine Zn(II) complexes. *J. Inorg. Biochem.* **2019**, *198*, 110727. [[CrossRef](#)]
11. Andelescu, A.A.; Cretu, C.; Sasca, V.; Marinescu, S.; Cseh, L.; Costisor, O.; Szerb, E.I. New heteroleptic Zn(II) and Cu(II) complexes with quercetine and N N ligands. *Polyhedron* **2018**, *147*, 120–125. [[CrossRef](#)]
12. Gusev, A.N.; Kiskin, M.A.; Braga, E.V.; Kryukova, M.A.; Baryshnikov, G.V.; Karaush-Karmazin, N.N.; Minaeva, V.A.; Minaev, B.F.; Ivaniuk, K.; Stakhira, P.; et al. Schiff Base Zinc(II) Complexes as Promising Emitters for Blue Organic Light-Emitting Diodes. *ACS Appl. Electron. Mater.* **2021**, *3*, 3436–3444. [[CrossRef](#)]
13. Di Bella, S.; Colombo, A.; Dragonetti, C.; Righetto, S.; Roberto, D. Zinc(II) as a Versatile Template for Efficient Dipolar and Octupolar Second-Order Nonlinear Optical Molecular Materials. *Inorganics* **2018**, *6*, 133. [[CrossRef](#)]
14. Di Bella, S. Lewis acidic zinc(II) salen-type Schiff-base complexes: Sensing properties and responsive nanostructures. *Dalton Trans.* **2021**, *50*, 6050. [[CrossRef](#)]
15. Consiglio, G.; Oliveri, I.P.; Failla, S.; Di Bella, S. On the Aggregation and Sensing Properties of Zinc(II) Schiff-Base Complexes of Salen-Type Ligands. *Molecules* **2019**, *24*, 2514. [[CrossRef](#)]
16. Diana, R.; Panunzi, B. The Role of Zinc(II) Ion in Fluorescence Tuning of Tridentate Pincers: A Review. *Molecules* **2020**, *25*, 4984. [[CrossRef](#)]
17. Hens, A.; Rajak, K.K. Photophysical property vs. medium: Mononuclear, dinuclear and trinuclear Zn(II) complexes. *RSC Adv.* **2015**, *5*, 4219–4232. [[CrossRef](#)]
18. Qin, X.; Ji, Y.; Gao, Y.; Yan, L.; Ding, S.; Wang, Y.; Liu, Z. Zinc(II) and Nickel(II) Complexes Based on Schiff Base Ligands: Synthesis, Crystal Structure, Luminescent and Magnetic Properties. *Z. Anorg. Allgem. Chem.* **2014**, *640*, 462–468. [[CrossRef](#)]
19. Soliman, A.A.; Linert, W. Structural Features of ONS-Donor Salicylidene Schiff Base Complexes. *Monatsh. Chem.* **2007**, *138*, 175–189. [[CrossRef](#)]
20. Donzelli, A.; Potvin, P.G. Ti $^{\text{IV}}$ Complexes of Redox-Active Schiff Bases. *Eur. J. Inorg. Chem.* **2012**, *2012*, 741–750. [[CrossRef](#)]
21. Roy, N.; Sproules, S.; Weyhermüller, T.; Wieghardt, K. Trivalent Iron and Ruthenium Complexes with a Redox Noninnocent (2-Mercaptophenylimino)-methyl-4,6-di-tert-butylphenolate(2-) Ligand. *Inorg. Chem.* **2009**, *48*, 3783–3791. [[CrossRef](#)] [[PubMed](#)]
22. Roy, N.; Sproules, S.; Bothe, E.; Weyhermüller, T.; Wieghardt, K. Polynuclear Complexes Containing the Redox Noninnocent Schiff Base Ligand 2-[(E)-2-Mercaptophenylimino]methyl-4,6-di-tert-butylphenolate(2-). *Eur. J. Inorg. Chem.* **2009**, *2009*, 2655–2663. [[CrossRef](#)]
23. Sproules, S.; Kapre, R.R.; Roy, N.; Weyhermüller, T.; Wieghardt, K. The molecular and electronic structures of monomeric cobalt complexes containing redox noninnocent o-aminobenzenethiolate ligands. *Inorg. Chim. Acta* **2010**, *363*, 2702–2714. [[CrossRef](#)]

24. Kawamoto, T.; Nishiwaki, M.; Tsunekawa, Y.; Nozaki, K.; Konno, T. Synthesis and Characterization of Luminescent Zinc(II) and Cadmium(II) Complexes with N,S-Chelating Schiff Base Ligands. *Inorg. Chem.* **2008**, *47*, 3095–3104. [[CrossRef](#)] [[PubMed](#)]
25. Amirnasr, M.; Bagheri, M.; Farrokhpour, H.; Schenk, K.J.; Mereiter, K.; Ford, P.C. New Zn(II) complexes with N₂S₂ Schiff base ligands. Experimental and theoretical studies of the role of Zn(II) in disulfide thiolate-exchange. *Polyhedron* **2014**, *71*, 1–7. [[CrossRef](#)]
26. Asadizadeh, S.; Amirnasr, M.; Tirani, F.F.; Mansouri, A.; Schenk, K. DNA-BSA interaction, cytotoxicity and molecular docking of mononuclear zinc complexes with reductively cleaved N₂S₂ Schiff base ligands. *Inorg. Chim. Acta* **2018**, *483*, 310–320. [[CrossRef](#)]
27. Labisbal, E.; Garcia-Vazquez, J.A.; Gomez, C.; Macias, A.; Romero, J.; Sousa, A. The synthesis of zinc(II) complexes of 2-(2-mercaptophenyl)-iminophenol by electrochemical cleavage of a disulfide bond; the crystal structure of {(2,2'-bipyridine)[2-(2-mercaptophenyl)iminophenoxy]}zinc(II). *Inorg. Chim. Acta* **1993**, *203*, 67–72. [[CrossRef](#)]
28. Shafaatian, B.; Sedighe Mousavi, S.; Afshari, S. Synthesis, characterization, spectroscopic and theoretical studies of new zinc(II), copper(II) and nickel(II) complexes based on imine ligand containing 2-aminothiophenol moiety. *J. Mol. Struct.* **2016**, *1123*, 191–198. [[CrossRef](#)]
29. Patra, C.; Bhanja, A.K.; Sen, C.; Ojha, D.; Chattopadhyaya, D.; Mahapatra, A.; Sinha, C. Imine-functionalized thioether Zn(ii) turn-on fluorescent sensor and its selective sequential logic operations with H₂PO₄[−], DFT computation and live cell imaging. *RSC Adv.* **2016**, *6*, 53378–53388. [[CrossRef](#)]
30. Kim, Y.-I.; Yun, S.-J.; Hwang, I.-H.; Kima, D.-Y.; Kang, S.K. Bis(2-[(9H-fluoren-2-yl)methylidene]amino) phenolato-κ²N,O)zinc methanol disolvate. *Acta Crystallogr. Sect. E Crystallogr. Commun.* **2012**, *68*, m504–m505. [[CrossRef](#)]
31. Protasenko, N.A.; Baryshnikova, S.V.; Cherkasov, A.V.; Poddel'skii, A.I. Pentacoordinated Complexes of Triphenyltin(IV) with Bidentate N-Phenyl-o-iminophenols. *Russ. J. Coord. Chem.* **2022**, *48*, 478–486. [[CrossRef](#)]
32. Klementyeva, S.V.; Lukoyanov, A.N.; Afonin, M.Y.; Mörtel, M.; Smolentsev, A.I.; Abramov, P.A.; Starikova, A.A.; Khusniyarov, M.M.; Konchenko, S.N. Europium and ytterbium complexes with o-iminoquinonato ligands: Synthesis, structure, and magnetic behavior. *Dalton Trans.* **2019**, *48*, 3338–3348. [[CrossRef](#)] [[PubMed](#)]
33. Klementyeva, S.V.; Smolentsev, A.I.; Abramov, P.A.; Konchenko, S.N. Yttrium 3,5-di-tert-butyl-catecholates supported by 2,6-diisopropylphenyl substituted β-diketiminato. *Inorg. Chem. Commun.* **2017**, *86*, 154–158. [[CrossRef](#)]
34. Baryshnikova, S.V.; Bellan, E.V.; Poddel'sky, A.I.; Arsenyev, M.V.; Smolyaninov, I.V.; Fukin, G.K.; Piskunov, A.V.; Berberova, N.T.; Cherkasov, V.K.; Abakumov, G.A. Tin(IV) and antimony(V) complexes bearing catecholate ligand connected to ferrocene. Synthesis, molecular structure and electrochemical properties. *Eur. J. Inorg. Chem.* **2016**, *2016*, 5230–5241. [[CrossRef](#)]
35. Baryshnikova, S.V.; Bellan, E.V.; Poddel'sky, A.I.; Fukin, G.K.; Abakumov, G.A. The synthesis and structure of new tin(II) complexes based on ferrocenyl-containing o-iminophenols. *Inorg. Chem. Commun.* **2016**, *69*, 94–97. [[CrossRef](#)]
36. Hao, J.; Liu, L.-Z.; Dong, W.-K.; Zhang, J.; Zhang, Y. Three multinuclear Co(II), Zn(II) and Cd(II) complexes based on a single-armed salamo-type bisoxime: Syntheses, structural characterizations and fluorescent properties. *J. Coord. Chem.* **2017**, *70*, 1936. [[CrossRef](#)]
37. Dey, D.; Kaur, G.; Ranjani, A.; Gayathri, L.; Chakraborty, P.; Adhikary, J.; Pasan, J.; Dhanasekaran, D.; Choudhury, A.R.; Akbarsha, M.A.; et al. A Trinuclear Zinc–Schiff Base Complex: Biocatalytic Activity and Cytotoxicity. *Eur. J. Inorg. Chem.* **2014**, *2014*, 3350. [[CrossRef](#)]
38. Shmakova, T.O.; Garnovsky, D.A.; Lyssenko, K.A.; Ivakhnenko, E.P.; Simakov, V.I.; Vasil'chenko, I.S.; Uraev, A.I.; Burlov, A.S.; Antipin, M.Y.; Garnovsky, A.D.; et al. Chemical and electrochemical syntheses of the binuclear zinc and cadmium chelates based on the sterically hindered Schiff bases. *Russ. J. Coord. Chem.* **2009**, *35*, 657. [[CrossRef](#)]
39. Dong, W.-K.; Zhang, J.; Zhang, Y.; Li, N. Novel multinuclear transition metal(II) complexes based on an asymmetric Salamo-type ligand: Syntheses, structure characterizations and fluorescent properties. *Inorg. Chim. Acta* **2016**, *444*, 95. [[CrossRef](#)]
40. Kushvaha, S.K.; Arumugam, S.; Shankar, B.; Sarkar, R.S.; Ramkumar, V.; Mondal, K.C. Isolation and Characterization of Different Homometallic and Heterobimetallic Complexes of Nickel and Zinc Ions by Controlling Molar Ratios and Solvents. *Eur. J. Inorg. Chem.* **2019**, 2871. [[CrossRef](#)]
41. Dong, W.-K.; Li, X.-L.; Wang, L.; Zhang, Y.; Ding, Y.-J. A novel relay-sensor for highly sensitive and selective detection of Zn²⁺/Pic[−] and fluorescence on/off switch response of H⁺/OH[−]. *Sens. Actuators B* **2016**, *229*, 370. [[CrossRef](#)]
42. Griffiths, K.; Tsipis, A.C.; Kumar, P.; Townrow, O.P.E.; Abdul-Sada, A.; Akien, G.R.; Baldansuren, A.; Spivey, A.C.; Kostakis, G.E. 3d/4f Coordination Clusters as Cooperative Catalysts for Highly Diastereoselective Michael Addition Reactions. *Inorg. Chem.* **2017**, *56*, 9563. [[CrossRef](#)] [[PubMed](#)]
43. Addison, A.W.; Rao, T.N.; Reedijk, J.; van Rijn, J.; Verschoor, G.C. Synthesis, structure, and spectroscopic properties of copper(II) compounds containing nitrogen–sulphur donor ligands; the crystal and molecular structure of aqua[1,7-bis(Nmethylbenzimidazolyl)-2,6-dithiaheptane]copper(II) perchlorate. *J. Chem. Soc. Dalton Trans.* **1984**, *1984*, 1349–1356. [[CrossRef](#)]
44. Smolyaninov, I.V.; Poddel'sky, A.I.; Baryshnikova, S.V.; Kuzmin, V.V.; Korchagina, E.O.; Arsenyev, M.V.; Smolyaninova, S.A.; Berberova, N.T. Electrochemical transformations and evaluation of antioxidant activity of some Schiff bases containing ferrocenyl and (thio-)phenol, catechol fragments. *Appl. Organometal. Chem.* **2018**, *32*, e4121. [[CrossRef](#)]
45. Smolyaninov, I.V.; Burmistrova, D.A.; Arsenyev, M.V.; Almyasheva, N.R.; Ivanova, E.S.; Smolyaninova, S.A.; Pashchenko, K.P.; Poddel'sky, A.I.; Berberova, N.T. Catechol- and Phenol-Containing Thio-Schiff Bases: Synthesis, Electrochemical Properties and Biological Evaluation. *ChemistrySelect* **2021**, *6*, 10609–10618. [[CrossRef](#)]

46. Yam, V.W.W.; Pui, Y.-L.; Cheung, K.-K. Synthesis, Emission, and Electrochemical Properties of Luminescent Dinuclear Zinc(II) Chalcogenolate Complexes. Dynamic ^1H NMR Studies and X-ray Crystal Structure of $[(\text{bpy})\text{Zn}_2(\text{SC}_6\text{H}_4\text{-Cl-p})(\mu\text{-SC}_6\text{H}_4\text{-Cl-p})(\mu\text{-OAc})_2]$. *Inorg. Chem.* **2000**, *39*, 5741–5746. [[CrossRef](#)]
47. Ngan, T.-W.; Ko, C.-C.; Zhu, N.; Yam, V.W.W. Syntheses, Luminescence Switching, and Electrochemical Studies of Photochromic Dithienyl-1,10-phenanthroline Zinc(II) Bis(thiolate) Complexes. *Inorg. Chem.* **2007**, *46*, 1144–1152. [[CrossRef](#)] [[PubMed](#)]
48. Budnikova, Y.H.; Dudkina, Y.B.; Kalinin, A.A.; Balakina, M.Y. Considerations on electrochemical behavior of NLO chromophores: Relation of redox properties and NLO activity. *Electrochim. Acta* **2021**, *368*, 137578. [[CrossRef](#)]
49. Jimenez-Perez, V.M.; Camacho-Camacho, C.; Guizado-Rodriguez, M.; Noth, H.; Contreras, R. New hexacyclic binuclear tin complexes derived from bis-(3,5-di-tert-butyl-2-phenol)oxamide. *J. Organomet. Chem.* **2000**, *614–615*, 283–293. [[CrossRef](#)]
50. Gordon, A.J.; Ford, R.A. *The Chemist's Companion*; Wiley: New York, NY, USA, 1972; p. 541.
51. Xinga, A.; Zenga, D.; Chen, Z. Synthesis, crystal structure and antioxidant activity of butylphenol Schiff bases: Experimental and DFT study. *J. Mol. Struct.* **2022**, *1253*, 132209. [[CrossRef](#)]
52. Krause, L.; Herbst-Irmer, R.; Sheldrick, G.M.; Stalke, D. Comparison of silver and molybdenum microfocus X-ray sources for single-crystal structure determination. *J. Appl. Crystallogr.* **2015**, *48*, 3–10. [[CrossRef](#)] [[PubMed](#)]
53. Sheldrick, G.M. SHELXT-Integrated Space-Group and Crystal-Structure Determination. *Acta Crystallogr. A* **2015**, *71*, 3–8. [[CrossRef](#)]
54. Dolomanov, O.V.; Bourhis, L.J.; Gildea, R.J.; Howard, J.A.K.; Puschmann, H. OLEX2: A complete structure solution, refinement and analysis program. *J. Appl. Crystallogr.* **2009**, *42*, 339–341. [[CrossRef](#)]
55. Frisch, M.J.; Trucks, G.W.; Schlegel, H.B.; Scuseria, G.E.; Robb, M.A.; Cheeseman, J.R.; Scalmani, G.; Barone, V.; Mennucci, B.; Petersson, G.A.; et al. *Gaussian 09, Revision, D.01*; Gaussian, Inc.: Wallingford, CT, USA, 2009.
56. Perdew, J.P.; Ernzerhof, M.; Burke, K. Rationale for mixing exact exchange with density functional approximations. *J. Chem. Phys.* **1996**, *105*, 9982–9985. [[CrossRef](#)]
57. Carlo, A.; Barone, V. Toward reliable density functional methods without adjustable parameters: The PBE0 model. *J. Chem. Phys.* **1999**, *110*, 6158–6170. [[CrossRef](#)]
58. Tomasi, J.; Mennucci, B.; Cammi, R. Quantum mechanical continuum solvation models. *Chem. Rev.* **2005**, *105*, 2999–3093. [[CrossRef](#)]
59. Grimme, S.; Antony, J.; Ehrlich, S.; Krieg, H. A consistent and accurate ab initio parametrization of density functional dispersion correction (DFT-D) for the 94 elements H-Pu. *J. Chem. Phys.* **2010**, *132*, 154104. [[CrossRef](#)]
60. Grimme, S.; Ehrlich, S.; Goerigk, L. Effect of the damping function in dispersion corrected density functional theory. *J. Comput. Chem.* **2011**, *32*, 1456–1465. [[CrossRef](#)]